[CANCER RESEARCH 62, 5325–5335, September 15, 2002]

Alterations in Gene Expression Profiles during Prostate Cancer Progression: Functional Correlations to Tumorigenicity and Down-Regulation of Selenoprotein-P in Mouse and Human Tumors[1]

Alfonso Calvo, Nianqing Xiao, Jason Kang,[2] Carolyn J. M. Best, Isabel Leiva, Michael R. Emmert-Buck, Cheryl Jorcyk, and Jeffrey E. Green[3]

Laboratory of Cell Regulation and Carcinogenesis [A. C., J. K., J. E. G.], Laboratory of Pathology [C. J. M. B., I. L., M. R. E-B.], Molecular Statistics and Bioinformatics [N. X.,]; and National Cancer Institute, NIH, Bethesda, Maryland 20892; and Department of Biology, Boise State University, Boise, Idaho 83725 [C. J.]

ABSTRACT

To identify molecular changes that occur during prostate tumor progression, we have characterized a series of prostate cancer cell lines isolated at different stages of tumorigenesis from C3(1)/Tag transgenic mice. Cell lines derived from low- and high-grade prostatic intraepithelial neoplasia, invasive carcinoma, and a lung metastasis exhibited significant differences in cell growth, tumorigenicity, invasiveness, and angiogenesis. cDNA microarray analysis of 8700 features revealed correlations between the tumorigenicity of the C3(1)/Tag-Pr cells and changes in the expression levels of genes regulating cell growth, angiogenesis, and invasion. Many changes observed in transcriptional regulation in this *in vitro* system are similar to those reported for human prostate cancer, as well as other types of human tumors. This analysis of expression patterns has also identified novel genes that may be involved in mechanisms of prostate oncogenesis or serve as potential biomarkers or therapeutic targets for prostate cancer. Examples include the L1-cell adhesion molecule, metastasis-associated gene (MTA-2), Rab-25, tumor-associated signal transducer-2 (Trop-2), and *Selenoprotein-P*, a gene that binds selenium and prevents oxidative stress. Many genes identified in the Pr-cell line model have been shown to be altered in human prostate cancer. The comprehensive microarray data provides a rational basis for using this model system for studies where alterations of specific genes or pathways are of particular interest. Quantitative real-time reverse transcription-PCR for Selenoprotein-P demonstrated a similar down-regulation of the transcript of this gene in a subset of human prostate tumors, mouse tumors, and prostate carcinoma cell lines. This work demonstrates that expression profiling in animal models may lead to the identification of novel genes involved in human prostate cancer biology.

INTRODUCTION

PCa[4] is the most prevalent cancer among men in the Western world (1). Preneoplastic lesions, known as PIN, have been found in men as early as 20 years of age and are commonly observed in men >50 years of age (2). PIN lesions are thought to be precursors of invasive prostate cancer in which incidence significantly increases in the sixth decade of life (3). Aging, genetic factors, environmental carcinogens, and steroid hormone levels are factors that have been associated with the development of prostate cancer (4).

The development of PCa is a multistage process that involves alterations in the expression of genes related to cell cycle regulation, apoptosis, adhesion, motility, and angiogenesis (5–7). Despite the considerable efforts made in recent years to understand prostate tumorigenesis, the molecular mechanisms involved in initiation and progression remain largely unknown (7). The development of animal models for prostate cancer has been an important step for studying oncogenesis in the prostate and testing preventive or therapeutic agents. Transgenic mouse models in particular have been valuable for studying prostate cancer progression and response to therapies (8, 9).

Our lab previously developed the C3(1)/Tag transgenic model of prostate cancer (10) where the SV40-Tag is expressed under the regulatory control of the C3(1) component of the rat steroid binding promoter gene C3(1). The development of prostate lesions in C3(1)/Tag transgenic mice is predictable, with PIN lesions forming at about 2 months of age and the emergence of invasive carcinomas after about 7 months of age (11). Based upon the predictable progression of tumor development in this model, we were recently able to develop a series of cell lines from C3(1)/Tag mice at different cancer stages: a LG-PIN cell-line, designated Pr111; a HG-PIN cell line, Pr117; a primary invasive carcinoma cell line, Pr14; and two cell lines derived from lung metastases, Pr14C1 and Pr14C2. These cells maintain expression of T-antigen and pan-cytokeratin, confirming their epithelial origin (12, 13). The Pr111 cell line has previously been shown to be androgen dependent. Pr117 and the Pr14 cell line variants are androgen responsive but not androgen dependent (12, 13). The *in vivo* tumorigenicity of these cell lines in nude mice correlates to the type of lesion from which they were derived.

We now demonstrate that the tumorigenicity of the C3(1)/Tag-Pr cell lines correlates with rates of cell proliferation, vascularization, and invasive properties of the cell lines. Moreover, gene expression profiling has revealed that the degree of tumorigenicity can be correlated to numerous transcriptional changes of known and unknown genes. The expression of many of these genes has been shown to be altered during tumor progression in human prostate cancer, as well as other types of human cancers. We demonstrate for the first time that Selenoprotein-P (Se-P), a gene down-regulated in malignant C3(1)/Tag-Pr cells, is also down-regulated in a subset of human prostate tumors. This study demonstrates that the Pr-cell line model system for prostate tumor progression is useful for identifying molecular changes during prostate cancer progression that may be relevant to understanding human prostate cancer.

MATERIALS AND METHODS

Cell Culture

Pr111, Pr117, Pr14, Pr14C1, and Pr14C2 cells from early passages (5–10) were cultured in collagen-coated flasks (Corning, NY) in the primary cell culture medium mammary epithelial growth media (MEGM) (Bio-Whittaker, Walkersville, MD) supplemented with 2% FBS (Invitrogen, Carlsbad, CA) and 4 nM of the synthetic androgen mibolerone (Sigma, St. Louis, MO). A low percentage of FBS (2%) was used to help maintain the PIN-like characteristics of the Pr111 and Pr117 cells (14).

Received 3/12/02; accepted 7/19/02.

The costs of publication of this article were defrayed in part by the payment of page charges. This article must therefore be hereby marked *advertisement* in accordance with 18 U.S.C. Section 1734 solely to indicate this fact.

[1] 1: A. C. is supported by a Fulbright-Ministerio de Educaicón y Ciencia fellowship at NIH.

[2] Present address: Spectral Genomics, 8080 North Stadium Drive, Houston, TX 77054.

[3] To whom requests for reprints should be addressed, at Laboratory of Cell Regulation and Carcinogenesis, National Cancer Institute, NIH, Building 41, Room C629, 41 Library Drive, Bethesda, MD 20892. Phone: (301) 435-5193; Fax: (301) 496-8395; E-mail: jegreen@nih.gov.

[4] PCa, prostate cancer; PIN, prostatic intraepithelial neoplasia; LG-PIN, low-grade PIN; HG-PIN, high-grade PIN; FBS, fetal bovine serum; VEGF, vascular endothelial growth factor; EGF, epidermal growth factor; IGF, insulin-like growth factor; RT-PCR, reverse transcription-PCR; Se-P, Selenoprotein-P; MMP, matrix metalloproteinase; TIMP, tissue inhibitor of metalloproteinase; L1-CAM, L1 cell adhesion molecule; EST, expressed sequence Tag; AR, androgen receptor.

PC-3 and LNCaP cells were obtained from American Type Culture Collection and cultured in RPMI 1640 (Invitrogen) supplemented with 10% FCS, 1 mM sodium pyruvate, 10 mM HEPES buffer, 2 mM glutamine, 50 units/ml penicillin G sodium, and 50 μg/ml streptomycin.

In Vitro Growth Assay

Cells/well (10^4) were cultured in 6-well plates (Corning Incorporated, Corning, NY). Cell number was counted daily using a Neubauer hemocytometer chamber (Hausser Scientific, Horsham, PA). For this purpose, the culture medium was removed, cells were washed with PBS, and incubated with 2 ml of trypsin-EDTA (Invitrogen) for 7 min. After adding another 2 ml of complete media, 10 μl of the solution were placed onto the hemocytometer. Cells were counted daily for 5 days, and the data were expressed as number of cells/ml.

In Vivo Cell Growth in C3(1)Tag Mice

Five-to-6-month-old C3(1)/Tag male mice (5 animals/cell line) received s.c. injections in the flank region with 10^6 cells. C3(1)/Tag mice were used because wild-type mice in the FVB/N background reject the tumor cells. Cells were tested to confirm that they were pathogen free. All manipulations of mice were carried out in accordance with the guidelines of the Animal Care and Use Committee and in accordance with the procedures outlined in the guide for the Care and Use of Laboratory Animals. Tumor volume was monitored weekly until the tumors reached 1 cm^3 in size.

Invasion Assay

Twenty-four-well BD BioCoat Matrigel Invasion Chambers (Becton Dickinson, Bedford, MA) were used, following the manufacturer's protocol. Briefly, 5×10^4 cells were diluted in serum-free DMEM and plated onto either the control or the Matrigel-covered inserts. DMEM (0.75 ml) supplemented with 20% FBS was placed in the lower part of the wells as a chemoattractant for the cells plated on the inserts. After 22 h in culture, cells were removed from the upper surface of the insert by scrubbing with a cotton swab. Cells on the lower surface of the insert were fixed with 4% paraformaldehyde and stained with 0.1% crystal violet. Inserts were placed onto slides, mounted with VectaMount (Vector Laboratories, Burlingame, CA) and analyzed under a Zeiss Axioplan microscope. The percent invasion was determined by dividing the mean number of cells invading through the matrigel insert by the mean number of cells invading through the control insert $\times$ 100. The invasive cell line MDA-MB231 and the noninvasive cell line NIH 3T3 were used as positive and negative controls, respectively.

Human Prostate Tumor Samples

Tissues were obtained from patients undergoing radical prostatectomy and evaluated by a pathologist for staging. Samples included four normal specimens and tumors with Gleason score 5 ($n = 1$), 6 ($n = 3$), 7 ($n = 2$), 8 ($n = 3$), 9 ($n = 1$), and 10 ($n = 1$). All of the specimens were studied anonymously.

Protein Extraction, Western Blot, and ELISA Analysis

Cells were homogenized in radioimmunoprecipitation assay buffer containing proteinase inhibitors (1$\times$ PBS, 1% NP40, 0.5% sodium deoxycholate, 0.1% SDS, and 10 ug/ml phenylmethylsulfonyl fluoride) and then cleared by centrifugation at 10,000 $\times$ *g* for 10 min. Protein concentration was measured with the Bio-Rad Protein Assay (Bio-Rad, Hercules, CA). Samples were electrophoresed through 12% Tris-Glycine gels (Novex, San Diego, CA) and transferred to a nitrocellulose membrane (Novex). Primary polyclonal antibody against VEGF (Neomarkers, Fremont, CA) was used at a 1:200 dilution for 2 h at room temperature. Secondary antibody (antirabbit IgG-horseradish peroxidase; Santa Cruz Biotechnology, Santa Cruz, CA) was used at 1:4000 dilution for 1 h. Detection of labeled antibodies was performed by chemoluminescence (NEN Life Science Products, Boston, MA).

Protein levels of VEGF were measured in cell lysates and supernatants by enzyme-linked immunoassay (Quantikine; R&D Systems, Minneapolis, MN). Each sample was incubated in triplicate wells in a microplate coated with anti-VEGF polyclonal antibody. After incubation and washing of the unlabeled proteins, peroxidase-linked anti-VEGF polyclonal antibody was added. After incubation for 2 h and washing, the enzymatic reaction was developed with H_2O_2 and tetramethylbenzidine. The reaction was stopped with HCl and absorbances were read at 450 nm on a Multiskan plate reader. VEGF concentrations were normalized to total protein concentrations.

Histology and Immunohistochemistry

C3(1)/Tag mice were euthanized by CO_2 asphyxiation, and tissues were immediately removed. Tumors were cut into several pieces. For RNA and protein analysis, samples were snap frozen in liquid nitrogen. Pieces of tumors, lungs, liver, and bone (close to the region in which the cells were injected) were fixed in 4% paraformaldehyde, and embedded in paraffin for histological examination. Four-μm sections were cut and stained with H&E. For CD-31 immunohistochemistry, samples were immediately immersed in optimal cutting temperature (OCT) compound (Tissue-Tek, Sakura, Japan) and frozen on a mixture of dry ice and isopentane (Fluka, St. Louis). Cryostat-cut sections were immersed in citric acid (pH 6) and heated in a microwave oven twice for 5 min for antigen retrieval. Slides were stained with anti-CD-31 antibody (PharMingen, San Diego, CA) at a 1:100 dilution. The avidin-biotin complex method (Vectastatin ABC Elite kit; Vector Laboratories) was used to visualize the bound antibodies. Negative controls were performed by omission of the primary antibody. For quantification of CD-31 staining, 30 fields randomly chosen were examined using a Zeiss Axoplan microscope, and images were captured and saved with Image Proplus software (Media Cybernetics, L.P.). CD-31-positive areas were selected and filtered. Data were given as relative area occupied by the CD-31 staining (vascular area) with respect to total area of the tumor.

cDNA Microarray Analysis

RNA Extraction, Preparation of the cDN-labeled Probes, and Hybridization. The Incyte mouse GEM1 set of cDNA clones containing 8700 features was arrayed on polylysine coated glass slides at the National Cancer Institute Advanced Technology Center. The gene list is available on line.[5]

Total RNA was extracted from frozen tissues using the RNeasy mini kit (Qiagen, Valencia, CA) according to the manufacturer's protocol. The quality of the RNA was assessed by running aliquots on agarose gels.

RNA from the minimally tumorigenic PIN cell line Pr111 was used as the common reference RNA in the competitive hybridizations of the microarray experiments against which the progressively tumorigenic Pr117, Pr14, Pr14C2, and Pr14C1 cell lines were compared. Preparation of the cDNA-labeled probes was performed using the Micromax system (NEN Life Science Products), according to the manufacture's protocol. Briefly, 10 μg of RNA from both the reference sample (Pr111) and the experimental samples were reverse transcribed for 1 h at 42°C using Cyanine 3-dUTP for the reference cell line Pr111 or Cyanine 5-dUTP for the experimental samples. Reference and experimental cDNA probes were mixed in equal amounts. The probe mix was filtered through an Amicon YM-30 purification system to eliminate the unincorporated nucleotides. After two washes with 10 mM Tris (pH 8)-1 mM EDTA, the labeled cDNA mixture was filter concentrated to a final volume of 7 μl, to which 1 μl (10 μg) of COT-1 DNA (Invitrogen), 1 μl (10 μg) of Poly-A (Amersham Pharmacia Biotech), and 1 μl (4 μg) of yeast tRNA (Sigma) were added for a final volume of 10 μl. An equal volume of 2$\times$ hybridization solution (50% formamide, 10$\times$ SSC, and 0.2% SDS) was added to the cDNA mixture and placed onto the microarray slide for hybridization at 42°C for 16 h.

Before the hybridization, slides were prehybridized with a solution consisting of 5$\times$ SSC, 0.1% SDS, and 1% BSA for 1 h at 42°C. Slides were then cleared in H_2O and isopropanol and dried by centrifugation (3 min, 550 rpm). After hybridization, slides were washed sequentially in a series of solutions with increasing stringency: 2$\times$ SSC, 0.1% SDS (solution A); 1$\times$ SSC, 0.1% SDS (solution B); 0.5$\times$ SSC (solution C); and 0.01$\times$ SSC (solution D). Immediately after the washing, slides were scanned with an Axon 4000B fluorescence laser-scanning instrument with a resolution of 10 μm (Axon Instruments, Foster City, CA).

Five separate hybridizations were performed for cell lines using Pr111 as a reference. To discard systematic errors because of dye incorporation, three extra reverse-fluorescence labelled microarray analyses were performed. In these cases, Pr111 cDNA (reference) was labeled with Cy-5, whereas Pr14C2, Pr117, and Pr14C1 cDNAs were labeled with Cy-3. Extensive analysis of

[5] Internet address: nciarray.nci.nih.gov.

reverse-fluorescence labelled labeling in our lab using the same arrays has revealed that dye bias is insignificant (15).

Data Filtering, Normalization, Clustering, and Statistical Analysis. Image analysis and the calculation of average foreground signal adjusted for local channel-specific background were performed using the GenePix Pro 3.0 software. Statistical analyses of the microarray data were performed using the S+ package. Spots with signal intensities in both channels < 100 were excluded from consideration. If at least one channel had an intensity > 100, the intensity under 100 was set at 100. Each array was globally normalized to make the median value of the log2-ratio equal to zero. This corrects for dye bias, photo multiplier tube (PMT) voltage imbalance, and variations between channels in amounts of samples hybridized. Hierarchical clustering of samples was based on a Pearson's correlation similarity metric. The results of hierarchical clustering are represented by a dendrogram.

Genes differentially expressed among cell lines were selected with magnitude of differences in geometric means of ratios as well as statistical significance based on student *t* test as criteria. Each of the four prostate tumor cell lines (Pr117, Pr14, Pr14C2, and Pr14C1) was compared with the PIN-like cell line Pr111. Genes with geometric means of ratios either >2 or <0.5 were first identified. Student *t* tests were then performed for each gene, and the *P*s were presented. The four tumor cell lines were also compared with each other in a similar fashion. For each pair of cell lines among the four, genes with at least a 2-fold difference in the geometric mean of ratios were identified. Student *t* tests were performed for each gene, and the *P*s were reported.

Quantitative Real-Time RT-PCR Analysis. Six μg of total RNA were incubated with DNaseI (Invitrogen) for 20 min. Reverse transcription was performed with the High Capacity cDNA archive kit (Applied Biosystems, Foster City, CA) according to the manufacturer's protocol. PCR primers targeting mouse androgen receptor, mouse and human Se-P, mouse IGF-BP3, and 28S rRNA were designed using Vector NTI software and are listed in Table 1. All of the primers were synthesized by Midland Certified Reagent Co. (Midland, TX). To assure the specificity of each primer set, amplicons generated from the PCR reaction were analyzed by determining their respective specific melting point temperature and additionally run on agarose gels to confirm the correct size of the PCR products. Quantitative analysis of gene expression was performed using Sybr PCR Core Reagents (PE Biosystems) and a Bio-Rad I-Cycler IQ Real-time detection system. Selected bacterial clones containing ESTs identical to the features of interest identified through array analyses were obtained from Incyte Genomics (Palo Alto, CA). Plasmids were purified from bacteria using the miniprep kit (Qiagen) and used as positive controls for the real-time RT-PCR analyses. In the case of androgen receptor, which was not represented on the microarray, a plasmid containing the mouse AR sequence, generously provided by Dr. Adam Adler, was used as a control. All assays were performed in triplicate.

RESULTS

Morphology and Cell Growth of C3(1)/Tag-Pr-cells. Fig. 1(*A–G*) illustrates the morphology of the C3(1)/Tag-Pr cell lines and the type of prostate lesions in C3(1)/Tag mice from which they were derived. Pr111 cells were isolated from a young mouse with LG-PIN characterized by focal pilling up of cells with an increase in epithelial cell number and cell density (Fig. 1*A*). Pr111 cells contained abundant cytoplasm, had elongated nuclei, and exhibited thin, cellular processes when cultured in collagen-coated flasks (Fig. 1*D*). Pr117 was developed from a stage of HG-PIN that contains numerous cells in a stratified pattern surrounded by an intact basement membrane (Fig. 1*B*). Cellular atypia with increased chromatin condensation and clumping is observed in HG-PIN (Fig. 1*B*). The Pr14 cell lines were isolated from a primary prostate tumor (Pr-14, Fig. 1*C*) or from lung metastasis derived from Pr14 (Pr14C1 and Pr14C2, Fig. 1*G*). The primary carcinoma exhibits cellular pleomorphism, including nuclear irregularity with prominent nucleoli, and invasion into the stroma. The Pr14 series of cell lines was smaller with less cytoplasm compared with Pr111 cells (Fig. 1*F*). The size and amount of cytoplasm of Pr117, the cell line isolated from an animal during the stage of HG-PIN formation (Fig. 1*B*), was intermediate between Pr111 and Pr14-derived cells (Fig. 1*E*). Each of the cell lines expressed cytokeratins specific for epithelial cells but not vimentin (12, 13), confirming their epithelial origin.

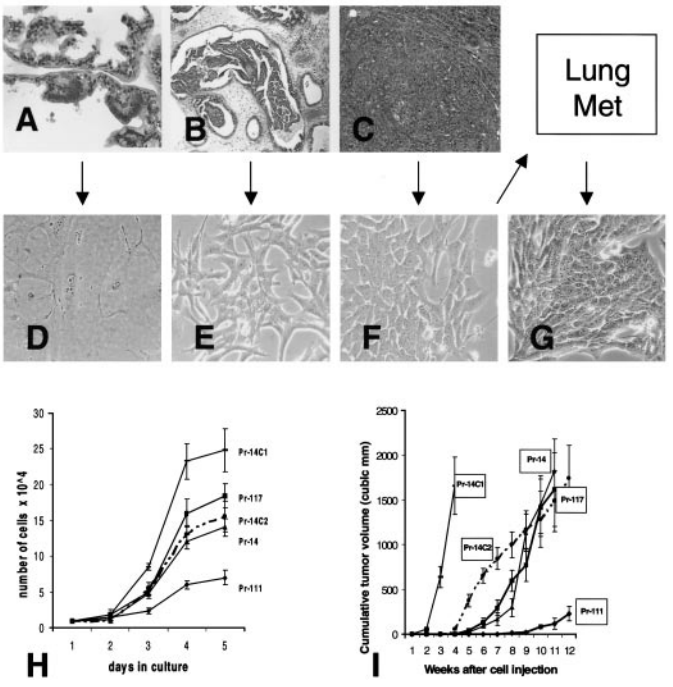

Fig. 1. Morphological features and growth rates of C3(1)/Tag cell lines. *Top and middle panels*, histology of the same type of prostate lesion from which the C3(1)/Tag cell lines were isolated and morphological features of the cells in culture. *A*, LG-PIN-like lesions in the prostate of a 3–4-month-old C3(1)/Tag mouse. *D*, Pr111 cells in culture, isolated from a prostate with LG-PIN-like lesions. *B*, HG-PIN-like lesions in the prostate of a 5-month-old C3(1)/Tag mouse from which the Pr117 line is derived. *E*, Pr117 cells in culture. *C*, adenocarcinoma in the prostate of a C3(1)/Tag mouse. *F*, morphology of Pr14 cells in culture isolated from a C3(1)/Tag mouse adenocarcinoma. Cells are small and lack cytoplasm processes compared with Pr111 and Pr117. Pr14C1 and Pr14C2 cells were isolated from lung metastasis found in nude mice after injection of Pr14. *G*, Pr14C1 cells in culture. *H*, growth rates of Pr-cell lines *in vitro*. Pr111 has the lowest rate of proliferation, whereas Pr14C1 has the highest rate of proliferation, with the other cells lines having intermediate rates. *I*, growth rates *in vivo* correlate with *in vitro* results.

The cell lines could be distinguished by their growth characteristics, both *in vitro* (Fig. 1*H*) and *in vivo* (Fig. 1*I*). Compared with the other cell lines, the LG-PIN cell line Pr111 had the lowest *in vitro* rate of proliferation (Fig. 1*H*) as well as *in vivo* tumor growth rate when injected s.c. into C3(1)/Tag male mice (Fig. 1*I*). The growth rates of Pr117, Pr14, and Pr14C2 were generally similar both *in vitro* (Fig. 1*H*) and *in vivo* (Fig. 1*I*) being intermediate between the growth rates of Pr111 and Pr14C1, which was clearly the most aggressive cell line. Only three of five mice that received injections of Pr111 cells developed tumors, which were small ($\leq$200 mm^3) 10–11 weeks after injection, whereas injection of all of the other cell lines produced large tumors that grew rapidly in five of five mice between 2 and 6 weeks after injection. Pr14C1 cells were the most aggressive and led to the

Table 1 *Primers used for quantitative real-time RT-PCR*

mIGF-BP3 sense (5′-3′)	AGG-GTG-TGT-GAG-TGT-GGT-GA
mIGF-BP3 antisense (5′-3′)	GCT-TTT-TGT-TGA-CTA-CTG-GG
mAR sense (5′-3′)	CCA-CTG-AGG-ACC-CAT-CCC-AGA-A
mAR antisense (5′-3′)	CGG-CAC-ACA-CCA-CTC-CTG-GCT-C
mSe-P sense (5′-3′)	GTC-TTC-CCT-CAG-TAA-GTA-CT
mSe-P antisense (5′-3′)	CTT-CTC-CAC-ATT-GCT-GAG-GT
hSe-P sense (5′-3′)	GAT-GGA-GCA-ACT-GAA-AGG-TG
hSe-P antisense (5′-3′)	CCC-CTA-GGT-CAT-AGT-TTA-CG
m/h 28S sense (5′-3′)[a]	GGG-TGG-TAA-ACT-CCA-TCT-AA
m/h 28S antisense (5′-3′)	AGT-TCT-TTT-CAA-CTT-TCC-CT

[a] m, mouse; h, human.

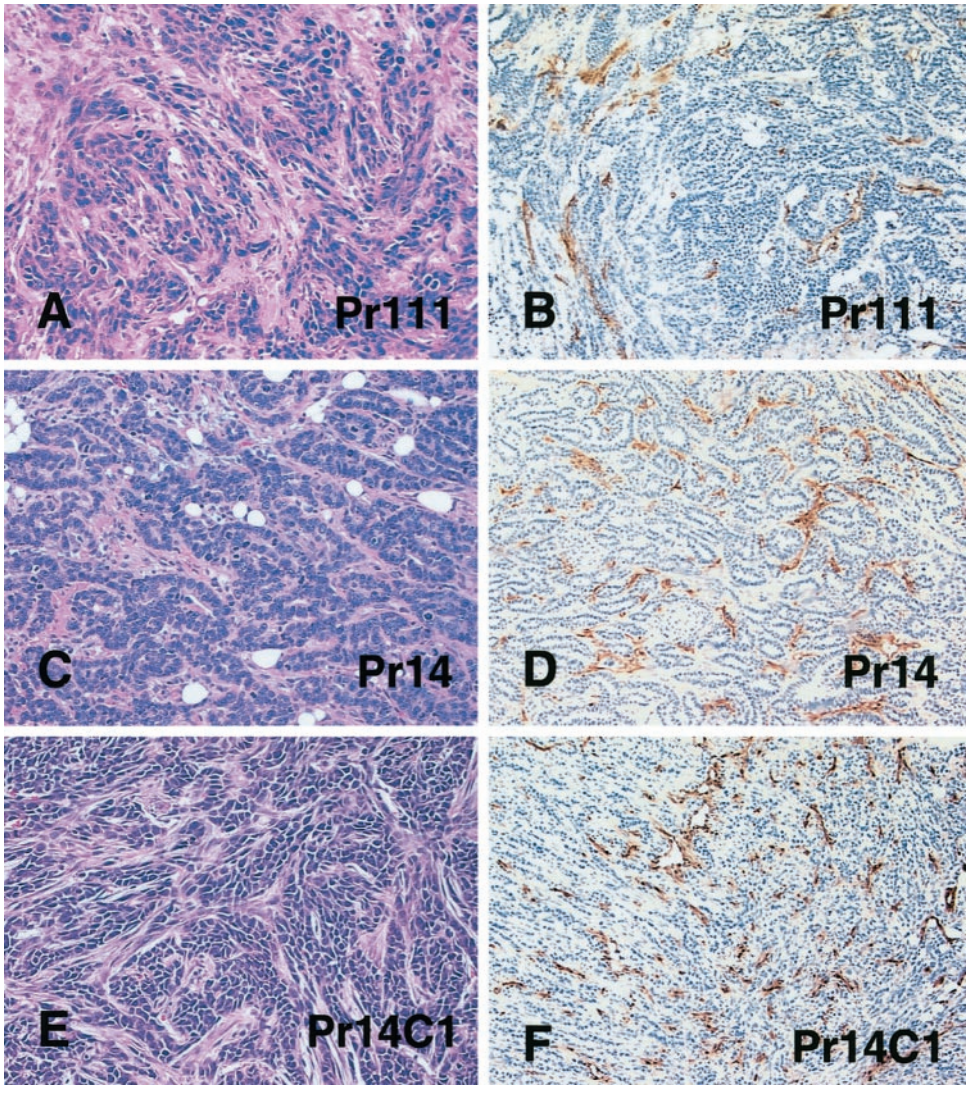

Fig. 2. Histological features of tumors from C3(1)/Tag-Pr cells injected s.c. into C3(1)/Tag male mice (*A*, *C*, *E*) with corresponding CD-31 immunostaining to assess vascularization (*B*, *D*, *F*). *A*, Pr111 cells occasionally develop small adenocarcinomas. *B*, CD-31 staining identifies blood vessels within tumors. *C*, Pr14 cells form adenocarcinomas with a well-differentiated glandular pattern. *D*, Pr14 tumors are more vascularized than tumors from Pr111. *E*, adenocarcinomas derived from Pr14C1 cells show nests of cells surrounded by fibrous stroma. *F*, tumors from Pr14C1 are highly vascularized.

development of large, palpable tumors within 4 weeks, requiring euthanasia of the animals.

The *in vitro* growth characteristics of the cell lines correlate well with the *in vivo* growth of tumors and establish a model system with a cell line of low tumorigenicity (Pr111), cell lines with intermediate tumorigenicity (Pr117, Pr14, Pr14C2) and a highly tumorigenic cell line (Pr14C1).

Differences in Tumor Vascularization and Angiogenesis in C3(1)/Tag-Pr Cells. We have assessed the ability of each C3(1)/Tag-Pr cell line to induce vascularization *in vivo*. The s.c. injection of these cell lines into mice resulted in adenocarcinomas with different degrees of vascularization and some differences in histological patterns. The small tumors generated from Pr111 cells demonstrated a moderate glandular pattern and were less vascularized than the tumors derived from the injection of the other C3(1)/Tag-Pr cells (Fig. 2, *A* and *B*). The percentage of area within the tumor occupied by vessels was determined by quantifying CD-31 staining. The relative area of vessels with respect to the total area of the tumor in Pr14, Pr14C1, and Pr14C2 cells ranged between 8.9 ± 2.1 and 12.5% ± 3.2 (without statistically significant differences), whereas for Pr111 tumors, the percentage of vessels was significantly lower (5.4% ± 1.%; $P < 0.05$). Tumors from Pr14 (Fig. 2, *C* and *D*) and Pr14C2 exhibited very similar histological features, including a well-differentiated glandular pattern with abundant vascularization. Tumors from Pr117 cells grew as poorly differentiated adenocarcinomas. The injection of Pr14C1 cells produced adenocarcinomas with nests of cells surrounded by fibrous stroma and a high degree of vascularization (Fig. 2, *E* and *F*).

Because VEGF is an important proangiogenic factor and was not represented on the microarrays we used, we determined the protein levels of VEGF produced by the C3(1)/Tag-Pr-cells. The LG-PIN cell line Pr111 expressed the lowest levels of VEGF protein, as demonstrated by Western blot (Fig. 3*A*) and by ELISA analyses of cell lysates and conditioned media (Fig. 3, *B* and *C*) compared with the other cell lines. This corresponds to the degrees of vascularization observed *in vivo* (Fig. 2). The HG-PIN cell line Pr117 had levels of VEGF intermediate between those of the Pr111 cells and the Pr14 cells. The highest VEGF levels were found in Pr14C1, although this was not statistically different from the levels of Pr14 or Pr14C2 cells (Fig. 3, *B* and *C*). The levels of VEGF were significantly higher in Pr14C1, Pr14C2, Pr14, and Pr117 cells compared with the Pr111 cells ($P < 0.05$).

Differences in Invasiveness in C3(1)/Tag-Pr Cells. The invasive properties of C3(1)/Tag-Pr cells were assessed using an *in vitro* assay that simulates the *in vivo* processes of cell detachment and movement through the basement membrane. Pr111 cells exhibited a very low level of invasiveness (<10%), compared with Pr117, Pr14, and Pr14C2 cells (range, 29.6 ± 8–38.7% ± 12; $P < 0.05$). Pr-14C1 cells

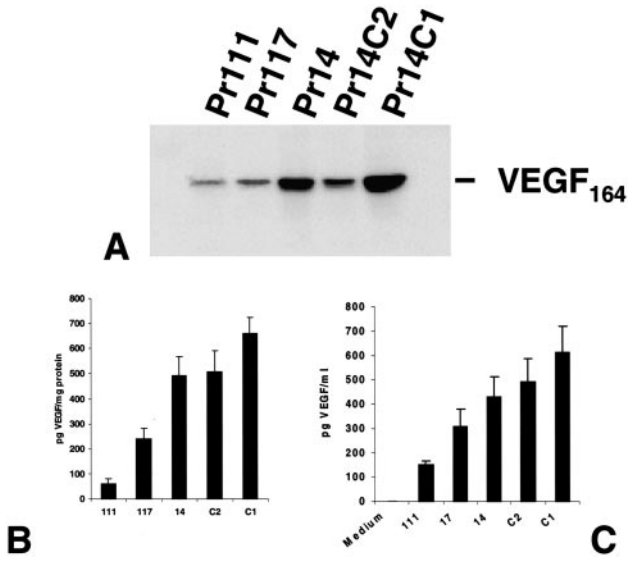

Fig. 3. VEGF protein expression in Pr-cell lines. *A*, Western blot of C3(1)/Tag-Pr cell lysates reveals a single band of M_r 23,000 corresponding to VEGF164. Pr14, Pr14C2, and Pr14C1 cells produce the highest amounts of VEGF. *B*, ELISA analysis for VEGF. Pr111 contains the lowest levels of VEGF, whereas Pr14C1 has the highest values. *C*, ELISA analysis for VEGF in conditioned media from Pr-cells corresponds to that for cell lysates.

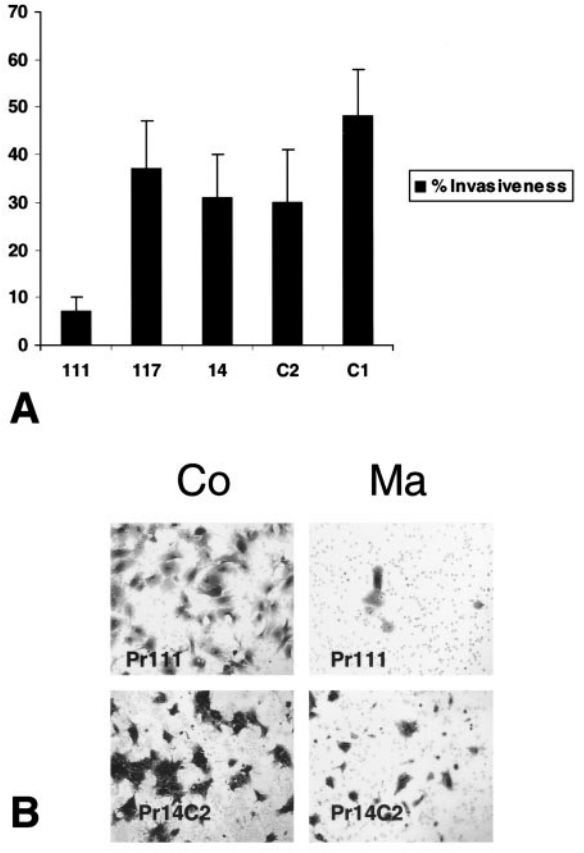

Fig. 4. Invasive properties of Pr-cells *in vitro* as determined by cell invasion assay. *A*, the LG-PIN cell line Pr111 exhibited the lowest invasive ability, whereas Pr117, Pr14, Pr14C2, and Pr14C1cells have significantly higher invasive properties than Pr111 ($P < 0.05$). The metastatic cell line Pr14C1 was the most invasive. *B*, representative microscopic fields of the filters used for the invasion analysis for Pr111 and Pr14C2. Very few invasive cells are observed in the Matrigel-coated filter (Ma) for Pr111 cells compared with the uncoated control filter (Co). The ratio of invasiveness for Pr4C2 is significantly higher than that for Pr111.

showed the highest degree of invasiveness (48.3% ± 13), correlating to the aggressive behavior of this cell line *in vivo* (Fig. 4). We have previously observed that only Pr14C2 and Pr14C1 were able to produce micrometastasis to the lungs when 5×10^5 cells were injected s.c. into nude mice, and animals were observed for at least 3 months.[6]

Gene Expression Profiling: Cluster Analysis. We have analyzed the relative expression levels of 8700 features represented on our arrays in an attempt to identify genes related to tumor progression in the Pr-cell line model of prostate tumor progression. RNA from the LG-PIN cell line Pr111 was used as the reference RNA in the competitive hybridizations with RNA from the more tumorigenic Pr-cell lines.

Hierarchical clustering was used to determine how the patterns of gene expression correlated between multiple samples from the individual C3(1)/Tag-Pr cell lines and between samples from all of the cell lines. Cluster analysis performed using all informative features within the array revealed that the Pr117 cells were grouped separately from the Pr14, Pr14C1, and Pr14C2 cells (Fig. 5*A*). The Pr14 series of cells clustered closely, as would be expected for cell lines derived from the same lineage. However, the PR14C1 cell line clustered separately from the Pr14 and Pr14C2 cell lines (Fig. 5*A*). The relationships defined by this cluster analysis are in keeping with the differences in biological properties of the cell lines as described above for cell growth, histology, invasiveness, and vascularization.

Using selection criteria where array expression values were increased or decreased to a minimum of 2-fold in at least 3 arrays/cell line, 325 genes were identified. Distinct differences in expression patterns of some genes were observed between the cell lines. Some of these differences may account for the more aggressive phenotype observed for the Pr14C1 cells compared with the Pr-14, Pr14C2, and Pr117 cells.

Cluster analysis revealed that a group of genes were progressively up-regulated from the LG-PIN-like cell line Pr117 to the malignant metastatic cell line Pr14C1 (Fig. 5*B*). These genes included cell adhesion molecules (adhesion lymphocyte antigen 6 and L1-CAM), metastasis-related genes (MTA-2) and genes related to cell cycle [c-myc, Rab-25, and transmembrane protein EGF-like (fibulin-4)] and the avian leukemia oncogene (p54). Another group of genes were exclusively up-regulated in Pr117 cells involving transcription factors (reticulocalbin and transcription factor-4) and oncogenes (Fyn proto-oncogene and MX-2; Fig. 5*B*).

Changes in Gene Expression Associated with Cell Growth. We have identified 467 genes differentially expressed (2-fold increase or decrease in expression; $P < 0.01$) between Pr111 and Pr117, 456 between Pr111 and Pr14, 420 between Pr111 and Pr14C2, and 516 between Pr111 and Pr14C1. Of these, ~90–100 genes were unknown ESTs. Known genes were classified (using GeneCards[7] and review of the literature) and grouped into three general categories: cell growth (including cell cycle, apoptosis, growth factors, transcription factors, signal transduction, and metabolism); angiogenesis; and metastasis. Fig. 6 shows examples of relevant changes in gene expression related to cell growth in the C3(1)/Tag-Pr cells. The expression of some genes that were differentially regulated between Pr111 cells and the other cell lines tended to progressively increase or decrease in expression according to the aggressiveness of each cell line. Examples of this type of pattern are shown for cyclin H, c-myc, Trop-2, tumor necrosis factor α-induced protein, annexin-II, metallothionein-1, and glutamine synthetase (Fig. 6). The levels of androgen receptor determined

[6] C. Jorcyk, unpublished data.

[7] Internet address: bioinformatics.weizmann.ac.il.

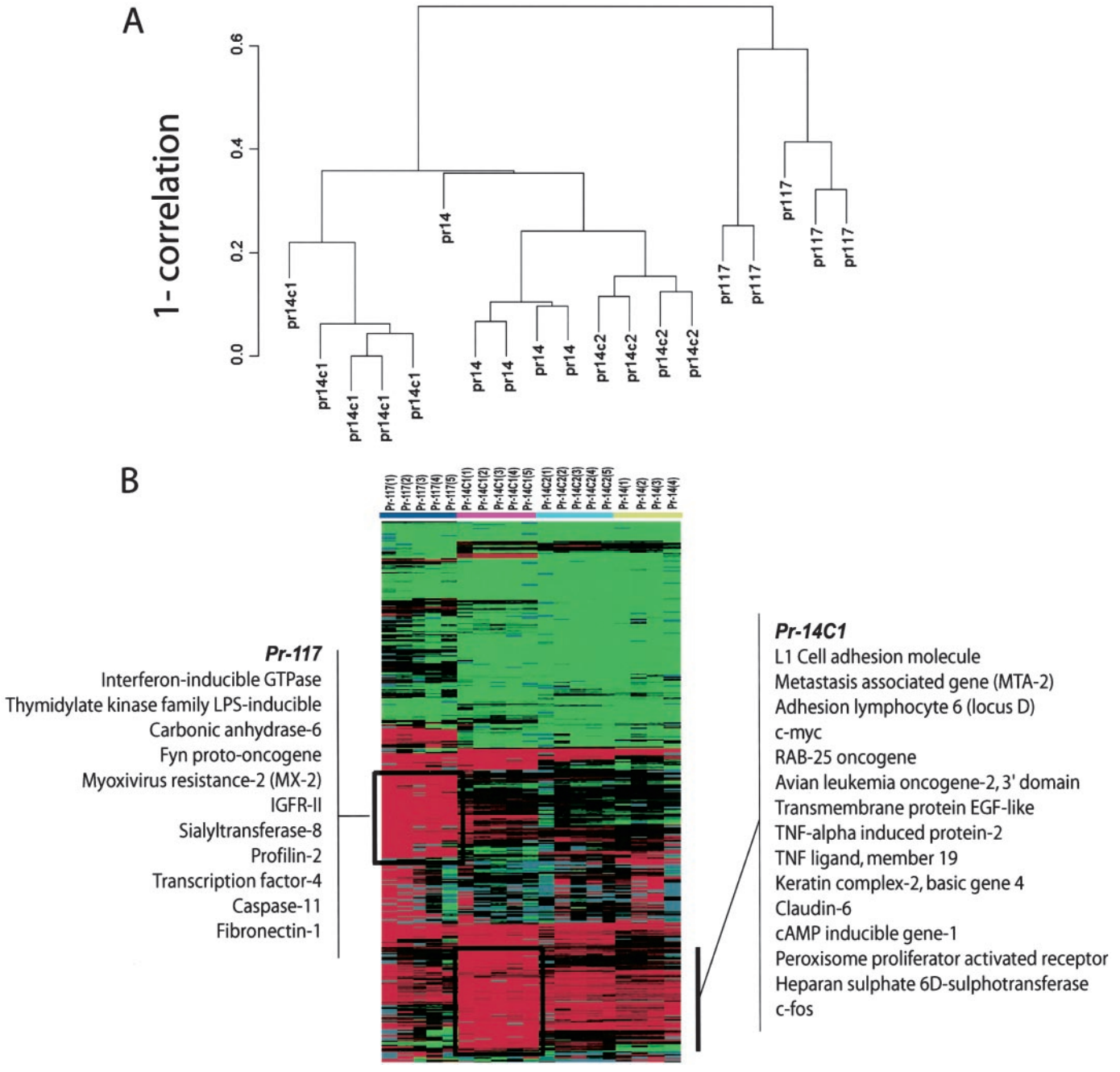

Fig. 5. Hierarchical clustering of gene expression for the Pr-cells. *A*, Pr117 clusters separate from the Pr14 cell lines with a low degree of correlation to the Pr14 cells. Pr14 and Pr14C2 cluster together, whereas PR14C1 clusters separate from the Pr14 and Pr14C2. *B*, a subset of genes specifically up-regulated in Pr117. A cluster of genes with increasing expression from HG-PIN cell line Pr117 to the metastatic cell line Pr14C1. Known genes strongly up-regulated in these clusters are listed. *Red* indicates up-regulation with respect to the internal reference Pr111, whereas *green* indicates down-regulation.

by RT-PCR decreased by ~3-fold in the cell lines derived from tumors or metastasis (Pr14, Pr14C1, and Pr14C2), compared with the Pr111 and Pr117 cells, which had similar values (results not shown).

Changes in Gene Expression Associated with Angiogenesis, Adhesion Molecules, and Invasion. Microarray analysis revealed numerous changes in the expression of genes related to angiogenesis and extracellular matrix modification between the LG-PIN-like cell line Pr111 and the more aggressive C3(1)/Tag-Pr cells. Examples of such up-regulated genes associated with increased tumorigenicity were MMP-2 and TIMP-3. Transglutaminase-2 was identified as a gene that was down-regulated (Fig. 7).

Our results also revealed decreased expression of adhesion molecules such as E-cadherin, N-cadherin, B-catenin, and adducin-3. Increased expression of P-cadherin, CEACAM-1, L1-CAM, adhesion lymphocyte-6 (locus D), metastasis-associated gene (*MTA-2*), and S100A8 were also associated with increased tumorigenicity (Fig. 7). The highest levels of expression of these metastasis-associated genes were observed in the metastatic cell line Pr14C1 (Fig. 7). A broader list of genes, including the average ratio and statistical comparisons, are available in Addendum Table 1 (http://rex.nci.nih.gov/research/basic/lc/jeg/ma/ac/table1.html).

Validation of cDNA Microarray Gene Expression Changes by Real-Time RT-PCR. We have previously demonstrated that a high correlation exists between the expression levels determined by mi-

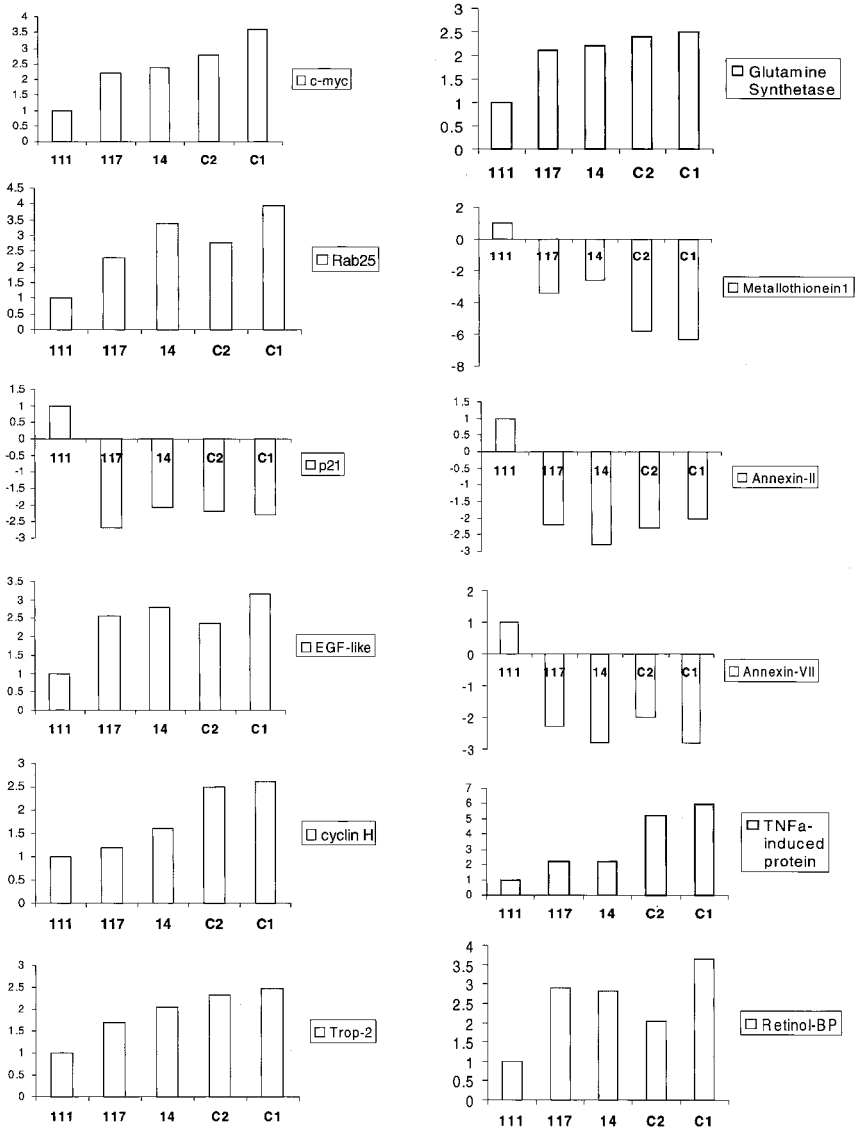

Fig. 6. Examples of gene expression changes associated with cell growth as revealed by microarray analysis. Y-axis represents the ratio of relative expression. C-myc, cyclin H, Trop-2, Rab-25, transforming growth factor α-induced protein, and glutamine synthetase are progressively up-regulated from the HG-PIN-like cell line Pr117 to the metastatic cell line Pr14C1. Examples of other up-regulated genes are EGF-like transmembrane protein and retinal binding protein. Examples of down-regulated genes are p21, metallothionein-1, annexin-II, and annexin-VII. Values are the average fold-change relative to the Pr111 cells. Each value represents RNA extracted from 4 to 5 independent cell cultures for each cell line. Differences between Pr111 and the other cell lines are statistically significant ($P < 0.05$).

croarray analysis and the RNA expression levels as determined by a Northern blot (15). To validate further the alterations in gene expression of two genes identified by microarray analyses with potential biological relevance to prostate cancer, primers were designed for real-time RT-PCR quantitation based upon the nucleotide sequence of the clones that were spotted onto the microarray. Two genes with opposite expression patterns were selected and analyzed: *Se-P*, found to be down-regulated in the highly tumorigenic Pr-cells; and *IGF-BP3*, found to be up-regulated in the highly tumorigenic Pr-cells. Sequence-verified clones of these genes were obtained from Incyte Genomics (Palo Alto, CA) and used as positive controls for the real-time RT-PCR analyses.

Gene expression patterns found by real time RT-PCR were very similar to those determined by microarray analysis for both genes (Fig. 8). Pr14C2 showed the highest levels of IGF-BP3. Although Se-P mRNA levels were significantly reduced in Pr14C1 cells both by real-time PCR and microarray analyses, the relative decrease was larger when determined by real time PCR compared with values obtained by microarray analyses (Fig. 8*B*). For all of the other cells, Se-P gene expression levels correlated well between the two techniques.

Correlation of Results to Changes in Human Prostate Cancer. Based upon the published literature, we have generated a list of genes with an expression that is similarly altered in the Pr-cell lines model of prostate cancer progression and human prostate cancer (Table 2). The expression of some genes in our *in vitro* system, however, was different from what has been reported in human prostate carcinoma (Table 2). We also identified genes with an expression that is significantly altered in our *in vitro* model but have not been studied in human prostate carcinoma. These genes, however, have been associated with other types of cancers. Examples of these genes include adducin-3, MTA-2, L1-CAM, and TIMP-3. Another set of genes identified in our *in vitro* model of tumor progression have not been previously associated with any human cancers and could potentially be considered as candidate markers for prostate cancer. Se-P is an example of such a gene. Se-P expression was also analyzed *in vivo* by real-time RT-PCR in tumors that developed after injection of the Pr-cell lines into mice and compared with levels found in normal mouse prostate tissue. Levels of Se-P mRNA were significantly decreased ($P < 0.05$) in tumors from Pr117, Pr14, Pr14C1, and Pr14C2 compared with normal prostate. A 5–8-fold decrease in expression in these tumors was observed in comparison with normal

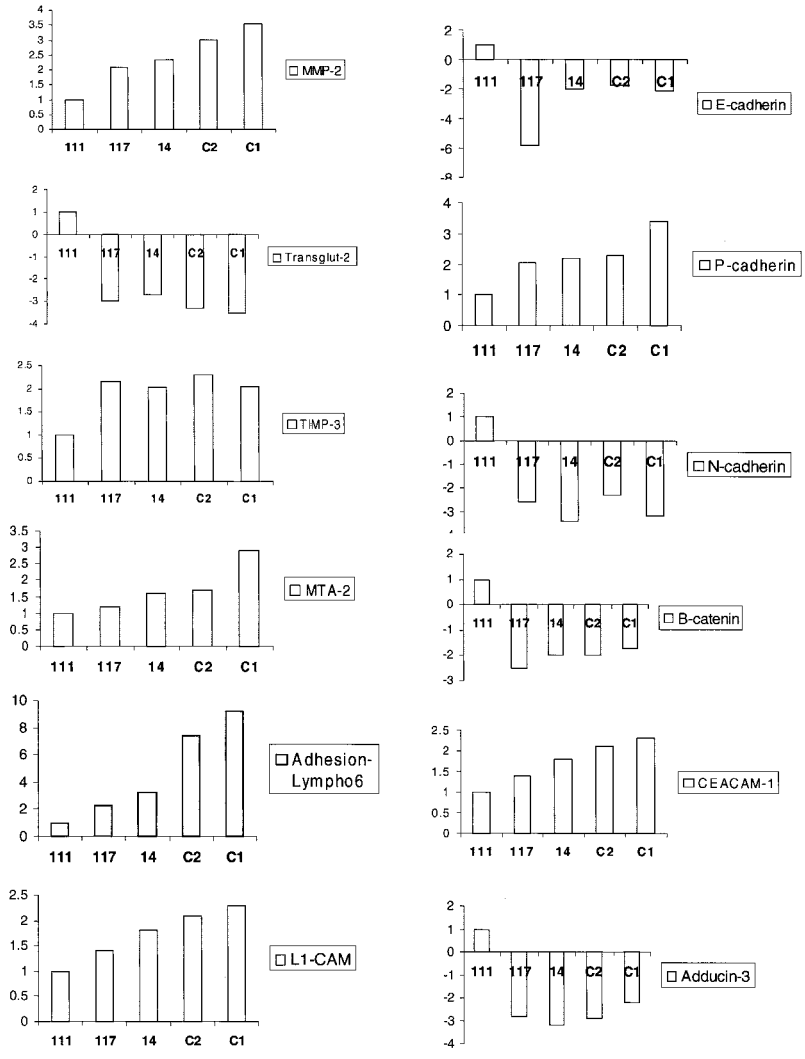

Fig. 7. Examples of gene expression changes associated with angiogenesis, adhesion molecules and invasion as determined by microarray analyses. MMP-2, Timp-3, MTA-2, adhesion lymphocyte-6, L1-CAM, P-cadherin, and CEACAM-1 are up-regulated during tumor progression whereas transglutaminase-2, E-cadherin, N-cadherin, B-catenin and adducing-3 are down-regulated. Values are the average fold-change relative to the Pr111 cells. Each value represents RNA extracted from 4–5 independent cell cultures for each cell line. Differences between Pr111 and the other cell lines are statistically significant ($P < 0.05$) and are listed in the Addendum Table 1.

prostate, with no statistical differences between types of tumors (data not shown).

Because low selenium has been associated with increased prostate cancer risk (33), we evaluated the expression of Se-P in normal human prostate tissue and human prostate cancer. Primers for real-time RT-PCR were designed to specifically amplify the human Se-P transcript (GenBank accession no. XM 011306). Results of real-time RT-PCR are summarized in Fig. 9. PCR products of samples were run on gels after 28 cycles of real-time RT-PCR (where there was a linear relationship between the amount of PCR product and the initial amount of cDNA). Fig. 9*B* shows a single band of the expected size (112 bp) found for both normal prostate and prostate carcinoma. Differential levels of expression between normal prostate and many tumor samples and the PCa cell lines were observed (Fig. 9*B*). The variability of Se-P levels was high in the prostate tumors, unlike that in the normal prostate (Fig. 9*A*). A subset of prostate tumors (7 of 11) had significantly lower levels of Se-P mRNA compared with normal prostate tissue. Four of the samples had a ~5-fold decrease, and three samples had a 2-fold decrease in Se-P levels compared with the normal prostate tissue. Other tumors ($n = 4$) had levels similar to the normal prostate. The levels of expression of Se-P in LNCaP and PC-3 were significantly decreased with respect to normal prostate. The reduction of Se-P in this subset of tumors was not because of degraded RNA as quality was assessed using the Agilent Bioanalyzer (Agilent Technologies, Palo Alto, CA), which revealed intact RNA. No statistically significant correlation between the mRNA levels of Se-P and Gleason grade was observed.

DISCUSSION

Prostate tumor progression results from alterations in the normal expression of genes related to the cell cycle, apoptosis, metabolism, adhesion, angiogenesis, and metastasis (5–7). To study these events in a well-defined *in vitro* system, we used our previously established cell line model system representing different stages of C3(1)/Tag-Pr prostate tumor progression (12, 13). These cell lines generated from C3(1)/Tag prostate tumors constitute the first *in vitro* model system representing different stages of prostate tumor progression in mice. Because these cell lines have been derived from mice that express the same transgene in an identical genetic background, they provide a unique system in which to study genetic changes that occur during tumor progression. Several *in vitro* human and mouse model systems exist for studying some aspects of prostate tumor progression, but these models are generally based upon cell lines derived from advanced tumors. Webber *et al.* (34) have recently reported the development of a series of human cell lines transformed by N-methyl-N-nitrosourea that may serve as a model for human prostate tumor progression.

We present evidence that the C3(1)/Tag cell lines represent various stages of tumor progression as measured by rates of cell proliferation,

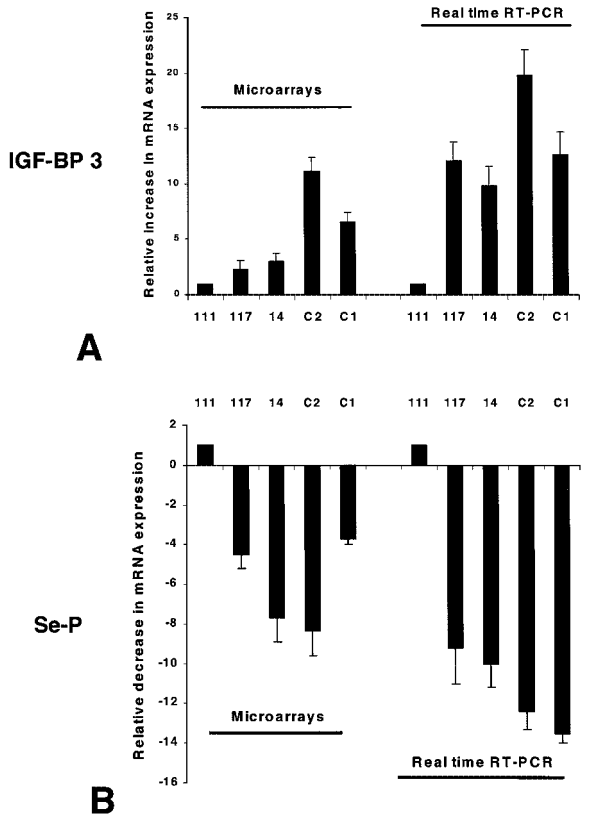

Fig. 8. Correlation between real-time RT-PCR and microarray results for IGF-BP3 and Se-P. Similar relative gene expression changes are observed using both techniques. IGF-BP3 (*A*) is increased in malignant cell lines, whereas Se-P (*B*) expression is down-regulated ($P < 0.05$; $n = 3$).

invasive properties, and tumorigenicity and vascularization in syngeneic mice. Results of the *in vitro* cell proliferation assay and the *in vivo* tumor growth of the Pr-cells show an increase in growth characteristics of the cells according to the stage of cancer at which the parental cell lines were obtained. The *in vivo* growth of the cells demonstrated that the Pr111 cells were not always tumorigenic, but when tumors grew they were the smallest and least vascularized tumors in contrast to the tumors produced by the more aggressive cell lines. Because the Pr-cell lines are rejected by normal FVB mice presumably because of the expression of Tag, we performed the tumorigenicity experiments in C3(1)/Tag mice with an intact immune system instead of nude mice. The invasive properties of the cells, as determined by the chamber migration assay, revealed that the most metastatic cell line, Pr14C1, invaded at a much higher rate compared with the other cell lines.

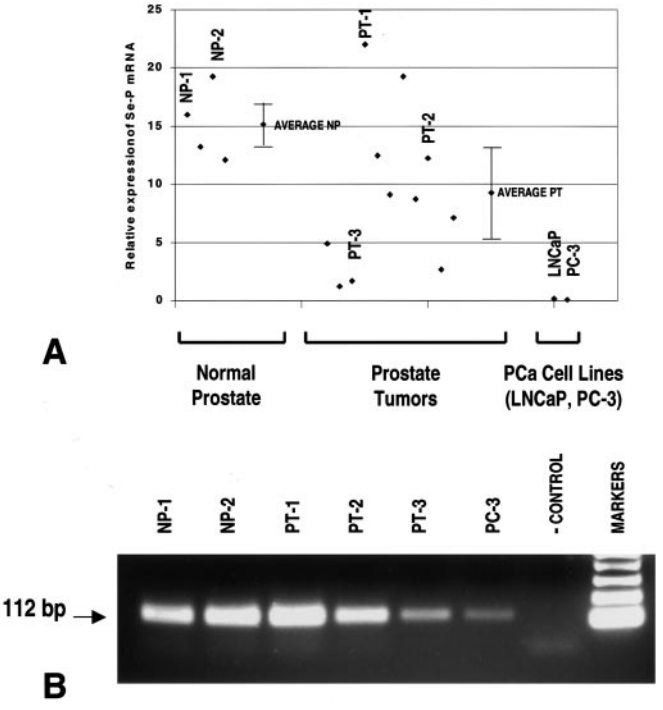

Fig. 9. Relative expression of Se-P in normal human prostates or human prostate carcinomas evaluated by real time RT-PCR. *A*, tumor samples show variable levels of Se-P expression compared with the normal prostates. A subset of tumor samples (7 of 11) have low levels of Se-P. Expression levels for the PCa cell lines LNCaP and PC-3 are markedly reduced with respect to the normal prostate. *B*, Se-P PCR products for human samples run on a 1% agarose gel after 28 cycles of PCR (where a linear correlation between PCR product and initial amounts of cDNA is observed). A single band of the expected size (112 bp) is observed for all of the samples. The expression of Se-P is down-regulated in tumor samples PT-2, PT-3, and in PC-3 cells. No band is seen in the negative control.

Table 2 *Gene expression status of selected genes in C3(1)/Tag cells and in human prostate carcinoma*

Gene	Status in malignant Pr-cells *versus* Pr111	Status in human PCa *versus* normal prostate
Genes similarly regulated in malignant C3(1)/Tag cells and in human prostate carcinoma		
Annexin II	Down-regulated	Down-regulated (16)
Annexin VII	Down-regulated	Down-regulated (17)
B-Catenin	Down-regulated	Down-regulated (18)
E-Cadherin	Down-regulated	Down-regulated (18, 19)
N-Cadherin	Down-regulated	Down-regulated (19)
c-myc	Up-regulated following a tumor progression pattern. Highly expressed in Pr14C1	Up-regulated (20)
EGF/EGF receptor	Up-regulated in relation to malignancy	Up-regulated (21)
IGF-BP3	Up-regulated during tumor progression. Highly expressed in Pr14C2	Up-regulated (22)
Metallothionein-1	Down-regulated during tumor progression. Very low expression in Pr14C2 and Pr14C1	Down-regulated (23)
MMP-2	Up-regulated	Up-regulated (24)
p21	Down-regulated	Down-regulated (25)
VEGF	Up-regulation in relation to malignancy	Up-regulated (26)
TIMP-2	Down-regulated	Down-regulated (24)
Tissue transglutaminase	Down-regulated	Down-regulated (27)
Genes dysregulated in C3(1)/Tag cells in which its expression in human PCa is variable with respect to normal prostate		
Androgen receptor	Down-regulated in tumor cells	Variable expression (28)
P-Cadherin	Down-regulated	Unclear (19, 29)
Genes differentially regulated in malignant C3(1)/Tag cells and in human prostate carcinoma		
CEACAM-1 (CD-66a)	Up-regulated during tumor progression. Highly expressed in Pr14C1	Down-regulated (30)
Cyclin D1	Down-regulated	Up-regulated (31)
IGF-RII	Up-regulated	Down-regulated (32)

There is also a correlation between the changes in gene expression patterns identified by cDNA microarray analyses and the biological properties of these cells. The cell line Pr111, derived at a stage of early LG-PIN, has the lowest *in vitro* growth rates and invasiveness, *in vivo* tumorigenicity, and vascularization compared with the cells derived from more advanced lesions. The Pr117 cell line, isolated from a more advanced stage of tumor progression (HG-PIN-like lesion), has intermediate characteristics between the LG-PIN-like cell line Pr111 and the tumor-derived cell lines in terms of cell morphology and expression levels of many genes such as VEGF, c-myc, MMP-2, L1-CAM, MTA-2, Trop-2, and cyclin H. However, invasiveness, tumor vascularization, and cell growth characteristics were similar to the tumor-derived cell lines. The metastatic cell line Pr14C1 demonstrates the most aggressive behavior, as evidenced by rapid *in vitro* and *in vivo* growth rates.

The aggressive properties of the Pr14C1 cell line are associated with the increased expression of several genes that may contribute to the accelerated growth and more invasive properties of these cells. Genes that could potentially contribute to the aggressive phenotype of Pr14C1 include CEACAM-1, L1-CAM, adhesion lymphocyte-6 (locus D), and the metastasis-associated gene *MTA-2*. Pr14C1 and Pr14C2 were able to form micrometastases to the lung in nude mice when 5×10^5 cells were injected s.c. 3 months after the injection (results not shown).

A subset of genes was identified whose levels of expression progressively increase or decrease in association with the degree of tumorgenicity of the cell lines. Examples of genes that follow this pattern are c-myc, Rab-25, avian leukemia oncogene, L1-CAM, and metastasis-associated gene *MTA-1*.

Interestingly, a substantial number of the differentially expressed tumor progression genes identified in our *in vitro* system are similarly dysregulated during human prostate oncogenesis. Examples of these include c-myc (20), MMP-2 (24) EGF (21), IGF-BP3 (22), and VEGF (26), which are overexpressed in most human prostate carcinomas. In contrast, E-cadherin (18, 19), p21 (25), metallothionein-1 (23), transglutaminase-2 (27), annexin II (16), and annexin VII (17) are commonly down-regulated in human prostate cancer and were similarly found to be reduced with advancing tumorigenicity of the C3(1)/Tag-Pr cell lines. Annexin II, also referred to as p36, is a calcium-binding protein involved in endocytosis, exocytosis, and membrane trafficking (35). Annexin VII is involved in cell growth, differentiation, motility, chemotaxis, and Ca 2+ availability (37). The annexin VII gene has been identified as an important tumor suppressor gene for prostate cancer (17). Many of these changes have also been observed in Tag-induced tumors in the transgenic model for prostate cancer (TRAMP) model.[8]

Several genes studied in our cell line model system, however, had expression patterns opposite to what has been described for human prostate cancer. Whereas cyclin D1 (32) is up-regulated, and IGF-RII (33) and CEACAM-1 (31) are down-regulated in human prostate cancer, we observed opposite expression patterns for these genes in the Pr-cell line model. The results presented in this work (and in supplementary material in the addendum) provide a rationale basis for determining what molecular similarities exist between this *in vitro* system and human prostate cancer. This information will be helpful in deciding when this model system may be appropriately used, depending upon the experimental question to be addressed.

Many of the genes we have found to be dysregulated in the C3(1)/Tag-Pr cells have not previously been reported to be aberrantly expressed in human or mouse prostate cancer. Several of the genes we have identified in this study have been associated with other types of tumors and demonstrate a similar expression pattern. Although more studies are required to determine the potential roles of these genes in human prostate cancer, some of these genes may represent biomarkers or possible novel therapeutic targets for prostate cancer. Examples of these novel genes up-regulated in relation to tumorigenicity are L1-CAM, metastasis-associated gene (*MTA-2*), lymphocyte antigen-6 (locus D), tumor-associated signal transducer (Trop-2), and Ras-related protein Rab-25. Examples of down-regulated genes are *TIMP-3*, *Se-P*, and *adducin-3*. Of particular interest are the adhesion/metastasis-associated genes L1-CAM and MTA-2, which have been implicated in tumor metastases (37, 38).

The down-regulation of Se-P may have biological significance in prostate oncogenesis. There is strong evidence that selenium has a significant protective effect against some types of cancers (33). Recent studies have reported that diet supplementation with selenium is associated with a significant decrease in cancer mortality and incidence (39). Selenium is a constituent of several major antioxidant enzymes, including glutathione peroxidase (GPX1), Se-P, gastrointestinal glutathione peroxidase (GPX2), and phospholipid hydroperoxide glutathione peroxidase (GPX4; Ref. 40). Se-P binds to ~60% of the selenium in plasma and has been found in several organs, including liver, heart muscle, kidney, lung, testis, and brain (40). It is thought that Se-P mediates two important functions: (*a*) the protection of tissues against oxidative stress; and (*b*) transport of selenium in serum and possible intracellular binding of selenium. Interestingly, Se-P levels are decreased by inflammatory activity (40), an event that often occurs during the initial stages of carcinogenesis (41). In rats with increased superoxide anion levels because of the injection of oxidative substances, selenium injection had a marked protective effect against lipid peroxidation and mortality (42, 43). Injection of selenium in plasma was followed by an increase in Se-P but not in glutathione peroxidase, indicating that Se-P itself may be a mediator of the protective effect of selenium (43). On the basis of these observations and our data, we speculate that administration of selenium might help prevent prostate tumor formation by up-regulation of Se-P, thus preventing the oxidative stress associated with carcinogenesis.

Considering these potentially important biological properties of Se-P in relation to oncogenesis, we evaluated Se-P expression in normal human prostate tissue and human prostate cancer by using quantitative real-time RT-PCR. We have described for the first time that both normal human prostate tissue and human prostate cancers express Se-P. However, levels of Se-P mRNA are significantly decreased in a subset of malignant carcinomas and in the androgen-dependent (LNCaP) and androgen-independent (PC-3) prostate cancer cell lines, compared with normal prostate tissue. The expression of this protein in tumors is quite variable, but in the majority of cases we have analyzed, expression was lower than in the normal prostate. Our results demonstrate that some cases of prostate cancer are accompanied by a down-regulation of Se-P, which could result in increased in oxidative stress. Our results suggest that reduced Se-P occurs in a subset of patients with a loss of protection against oxidative stress, but the potential clinical relevance of low Se-P in prostate cancer and Se supplementation require further study.

In summary, microarray analysis of the *in vitro* model system for prostate tumor progression derived from various stages of C3(1)/Tag prostate lesions has revealed molecular alterations that appear relevant to the study of human prostate cancer. The detailed understanding of which transcriptional changes occur in this unique model system provides a basis for rationally determining which pathways and molecular targets are appropriate for further study in this system. Comparisons between this *in vitro* system, tumors arising *in vivo* in

[8] J. E. Green, unpublished observations.

transgenic models and human prostate cancer will provide important insights into model characterization and credentialing.

ACKNOWLEDGMENTS

We thank Lisa Birely for technical assistance with the animals, Drs. John Powell and John Greene for array database support, and Drs. Anita Roberts and Kartiki Desai for review of this manuscript.

REFERENCES

1. Greenlee, R. T., Hill-Harmon, M. B., Murray, T., and Thun, M. Cancer Statistics, 2001. CA - Cancer J. Clin., *51:* 15–36, 2001.
2. Sakr, W. A., Haas, G. P., Cassin, B. F., Pontes, J. E., and Crissman, J. D. The frequency of carcinoma and intraepithelial neoplasia of the prostate in young male patients. J. Urol., *150:* 379–385, 1993.
3. Debre, B., Geraud, M., Flam, T., and Steg, A. Epidemiology of prostatic cancer. J. Int. Med. Res., *1:* 3–7, 1990.
4. Wild, C. P., Andersson, C., O'Brien, N. M., Wilson, L., and Woods, J. A. A critical evaluation of the application of biomarkers in epidemiological studies on diet and health. Br. J. Nutr., *86:* 37–53, 2001.
5. Culig, Z., Hobisch, A., Cronauer, M. V., Radmayr, C., Hittmair, A., Zhang, J., Thurnher, M., Bartsch, G., and Klocker, H. Regulation of prostatic growth and function by peptide growth factors. Prostate, *6:* 392–405, 1996.
6. Harper, M. E., Glynne-Jones, E., Goddard, L., Thurston, V. J., and Griffiths, K. Vascular endothelial growth factor (VEGF) expression in prostatic tumours and its relationship to neuroendocrine cells. Br. J. Cancer, *74:* 910–916, 1996.
7. Abate-Shen, C., and Shen, M. M. Molecular genetics of prostate cancer. Genes Dev., *14:* 2410–2434, 2000.
8. Green, J. E., Shibata, M. A., Shibata, E., Moon, R. C., Anver, M. R., Kelloff, G., and Lubet, R. 2-Difluoromethylornithine and dehydroepiandrosterone inhibit mammary tumor progression but not mammary or prostate tumor initiation in C3(1)/SV40 T/t-antigen transgenic mice. Cancer Res., *61:* 7449–7455, 2001.
9. Gupta, S., Ahmad, N., Marengo, S. R., MacLennan, G. T., Greenberg, N. M., and Mukhtar, H. Chemoprevention of prostate carcinogenesis by α-difluoromethylornithine in TRAMP mice. Cancer Res., *60:* 5125–5133, 2000.
10. Maroulakou, I. G., Anver, M., Garrett, L., and Green, J. E. Prostate and mammary adenocarcinoma in transgenic mice carrying a rat C3(1) simian virus 40 large tumor antigen fusion gene. Proc. Natl. Acad. Sci. USA, *91:* 11236–11240, 1994.
11. Shibata, M. A., Ward, J. M., Devor, D. E., Liu, M. L., and Green, J. E. Progression of prostatic intraepithelial neoplasia to invasive carcinoma in C3(1)/SV40 large T antigen transgenic mice: histopathological and molecular biological alterations. Cancer Res., *56:* 4894–4903, 1996.
12. Jorcyk, C. L., Liu, M. L., Shibata, M. A., Maroulakou, I. G., Komschlies, K. L., McPhaul, M. J., Resau, J. H., and Green, J. E. Development and characterization of a mouse prostate adenocarcinoma cell line: ductal formation determined by extracellular matrix. Prostate, *34:* 10–22, 1998.
13. Soares, C. R., Shibata, M. A., Green, J. E., and Jorcyk, C. L. Development of PIN and prostate adenocarcinoma cell lines: a model system for multistage tumor progression. Neoplasia, *4:* 112–120, 2002.
14. Peehl, D. M., and Stamey, T. A. Growth responses of normal, benign hyperplastic, and malignant human prostatic epithelial cells in vitro to cholera toxin, pituitary extract, and hydrocortisone. Prostate, *8:* 51–61, 1986.
15. Desai, K., Xiao, N., Wang, W., Gangi, L., Greene, J., Powell, J., Dickson, R., Furth, P., Hunter, K., Kucherlapati, R., Simon, R., Liu, E., and Green, J. Initiating oncogenic event determines gene expression patterns of human breast cancer models. Proc. Natl. Acad. Sci. USA, *99:* 6967–6972, 2002.
16. Chetcuti, A., Margan, S. H., Russell, P., Mann, S., Millar, D. S., Clark, S. J., Rogers, J., Handelsman, D. J., and Dong, Q. Loss of annexin II heavy and light chains in prostate cancer and its precursors. Cancer Res., *61:* 6331–6334, 2001.
17. Srivastava, M., Bubendorf, L., Srikantan, V., Fossom, L., Nolan, L., Glasman, M., Leighton, X., Fehrle, W., Pittaluga, S., Raffeld, M., Koivisto, P., Willi, N., Gasser, T. C., Kononen, J., Sauter, G., Kallioniemi, O. P., Srivastava, S., and Pollard, H. B. ANX7, a candidate tumor suppressor gene for prostate cancer. Proc. Natl. Acad. Sci. USA, *98:* 4575–4580, 2001.
18. Kallakury, B. V., Sheehan, C. E., and Ross, J. S. Co-down-regulation of cell adhesion proteins α- and β-catenins, p120CTN, E-cadherin, and CD44 in prostatic adenocarcinomas. Hum. Pathol., *32:* 849–855, 2001.
19. Arenas, M. I., Romo, E., Royuela, M., Fraile, B., and Paniagua, R. E-, N-, and P-cadherin and α-, β- and γ-catenin protein expression in normal, hyperplastic, and carcinomatous human prostate. Histochem. J., *32:* 659–667, 2000.
20. Latil, A., Vidaud, D., Valeri, A., Fournier, G., Vidaud, M., Lidereau, R., Cussenot, O., and Biache, I. htert expression correlates with MYC overexpression in human prostate cancer. Int. J. Cancer, *89:* 172–176, 2000.
21. Gil-Diez de Medina, S., Salomon, L., Colombel, M., Abbou, C. C., Bellot, J., Thiery, J. P., Radvanyi, F., Van der Kwast, T. H., and Chopin, D. K. Modulation of cytokeratin subtype, EGF receptor, and androgen receptor expression during progression of prostate cancer. Hum. Pathol., *29:* 1005–1012, 1998.
22. Khosravi, J., Diamandi, A., Mistry, J., and Scorilas, A. Insulin-like growth factor I (IGF-I) and IGF-binding protein-3 in benign prostatic hyperplasia and prostate cancer. J. Clin. Endocrinol. Metab., *86:* 694–699, 2001.
23. Garrett, S. H., Sens, M. A., Shukla, D., Flores, L., Somji, S., Todd, J. H., and Sens, D. A. Metallothionein isoform 1 and 2 gene expression in the human prostate: down-regulation of MT-1X in advanced prostate cancer. Prostate, *43:* 125–135, 2000.
24. Still, K., Robson, C. N., Autzen, P., Robinson, M. C., and Hamdy, F. C. Localization and quantification of mRNA for matrixmetalloproteinase-2 (MMP-2) and tissue inhibitor of matrix metalloproteinase-2 (TIMP-2) in human benign and malignant prostatic tissue. Prostate, *42:* 18–25, 2000.
25. Cheng, L., Lloyd, R. V., Weaver, A. L., Pisansky, T. M., Cheville, J. C., Ramnani, D. M., Leibovich, B. C., Blute, M. L., Zincke, H., and Bostwick, D. G. The cell cycle inhibitors p21WAF1 and p27KIP1 are associated with survival in patients treated by salvage prostatectomy after radiation therapy. Clin. Cancer Res., *6:* 1896–1899, 2000.
26. Kollermann, J., and Helpap, B. Expression of vascular endothelial growth factor (VEGF) and VEGF receptor Flk-1 in benign, premalignant, and malignant prostate tissue. Am. J. Clin. Pathol., *116:* 115–121, 2001.
27. Birckbichler, P. J., Bonner, R. B., Hurst, R. E., Bane, B. L., Pitha, J. V., and Hemstreet, G. P. Loss of tissue transglutaminase as a biomarker for prostate adenocarcinoma. Cancer (Phila.), *89:* 412–423, 2000.
28. Ruizeveld de Winter, J. A., Janssen, P. J., Sleddens, H. M., Verleun-Mooijman, M. C., Trapman, J., Brinkmann, A. O., Santerse, A. B., Schroder, F. H., and van der Kwast, T. H. Androgen receptor status in localized and locally progressive hormone refractory human prostate cancer. Am. J. Pathol., *144:* 735–746, 1994.
29. Paul, R., Ewing, C. M., Jarrard, D. F., and Isaacs, W. B. The cadherin cell-cell adhesion pathway in prostate cancer progression. Br. J. Urol., *79:* 37–43, 1997.
30. Luo, W., Tapolsky, M., Earley, K., Wood, C. G., Wilson, D. R., Logothetis, C. J., and Lin, S. H. Tumor-suppressive activity of CD66a in prostate cancer. Cancer Gene Ther., *6:* 313–321, 1999.
31. Drobnjak, M., Osman, I., Scher, H. I., Fazzari, M., and Cordon-Cardo, C. Overexpression of cyclin D1 is associated with metastatic prostate cancer to bone. Clin. Cancer Res., *6:* 1891–1895, 2000.
32. Mita, K., Nakahara, M., and Usui, T. Expression of the insulin-like growth factor system and cancer progression in hormone-treated prostate cancer patients. Int. J. Urol., *7:* 321–329, 2000.
33. Brown, K. M., and Arthur, J. R. Selenium, selenoproteins, and human health: a review. Public Health Nutr., *4:* 593–599, 2001.
34. Webber, M. M., Quader, S. T., Kleinman, H. K., Bello-DeOcampo, D., Storto, P. D., Bice, G., DeMendonca-Calaca, W., and Williams, D. E. Human cell lines as an *in vitro*/*in vivo* model for prostate carcinogenesis and progression. Prostate, *47:* 1–13, 2001.
35. Merrifield, C. J., Rescher, U., Almers, W., Proust, J., Gerke, V., Sechi, A. S., and Moss, S. E. Annexin 2 has an essential role in actin-based macropinocytic rocketing. Curr. Biol., *11:* 1136–1141, 2001.
36. Bonfils, C., Greenwood, M., and Tsang, A. Expression and characterization of a Dictyostelium discoideum annexin. Mol. Cell. Biochem., *139:* 159–166, 1994.
37. Matsusue, K., Takiguchi, S., Toh, Y., and Kono, A. Characterization of mouse metastasis-associated gene 2: genomic structure, nuclear localization signal, and alternative potentials as transcriptional activator and repressor. DNA Cell Biol., *20:* 603–611, 2001.
38. Voura, E. B., Ramjeesinghm, R. A., Montgomery, A. M., and Siu, C. H. Involvement of integrin $\alpha(v)\beta(3)$ and cell adhesion molecule L1 in transendothelial migration of melanoma cells. Mol. Biol. Cell, *12:* 2699–2710, 2001.
39. Clark, L. C., Combs, G. F., Jr., Turnbull, B. W., Slate, E. H., Chalker, D. K., Chow, J., Davis, L. S., Glover, R. A., Graham, G. F., Gross, E. G., Krongrad, A., Lesher, J. L., Jr., Park, H. K., Sanders, B. B., Jr., Smith, C. L., and Taylor, J. R. Effects of selenium supplementation for cancer prevention in patients with carcinoma of the skin. A randomized controlled trial. Nutritional Prevention of Cancer Study Group. J. Am. Med. Assoc., *276:* 1957–1963, 1996.
40. Moschos, M. P. Selenoprotein P. Cell Mol. Life Sci., *57:* 1836–1845, 2000.
41. Surh, Y. J., Chun, K. S., Cha, H. H., Han, S. S., Keum, Y. S., Park, K. K., and Lee, S. S. Molecular mechanisms underlying chemopreventive activities of anti-inflammatory phytochemicals: down-regulation of COX-2 and iNOS through suppression of NF-κB activation. Mutat. Res., *480:* 243–268, 2001.
42. Burk, R. F., Lawrence, R. A., and Lane, J. M. Liver necrosis and lipid peroxidation in the rat as the result of paraquat and diquat administration. Effect of selenium deficiency. J. Clin. Investig., *65:* 1024–1031, 1980.
43. Burk, R. F., Hill, K. E., Awad, J. A., Morrow, J. D., Kato, T., Cockell, K. A., and Lyons, P. R. Pathogenesis of diquat-induced liver necrosis in selenium-deficient rats: assessment of the roles of lipid peroxidation and selenoprotein P. Hepatology, *21:* 561–569, 1995.